Available online at www.sciencedirect.com
ScienceDirect
Deep-Sea Research I 54 (2007) 1390–1401
DEEP-SEA RESEARCH PART I
www.elsevier.com/locate/dsri

Instruments and Methods

Meridional heat transport determined with expendable bathythermographs—Part I: Error estimates from model and hydrographic data

Molly O. Baringer*, Silvia L. Garzoli

NOAA Atlantic Oceanographic and Meteorological Laboratory, Miami, FL 33149, USA

Received 1 November 2006; received in revised form 20 March 2007; accepted 26 March 2007
Available online 13 April 2007

Abstract

Heat transports estimated CTD data collected during the World Ocean Circulation Experiment (WOCE) along the January 1993 30°S hydrographic transect (A10) and the output from a numerical model show a mean heat transport of 0.40 and 0.55 ± 0.24 PW (standard deviation), respectively. The model shows a large annual cycle in heat transport (more than 30% of the variance) with a maximum (minimum) heat transport in July (February) of 0.68 (0.41) PW. Using these data, a method is proposed and evaluated to calculate the heat transport from temperature data obtained from a trans-basin section of expendable bathythermographs (XBTs) profiles. In this method, salinity is estimated from Argo profiles and CTD casts for each XBT temperature observation using statistical relationships between temperature, latitude, longitude and salinity computed along constant-depth surfaces. Full-depth temperature/salinity profiles are obtained by extending the profiles to the bottom of the ocean using deep climatological data. The meridional transport is then determined by using the standard geostrophic method, applying NCEP-derived Ekman transports, and requiring that the salt flux through the Bering Straits be conserved. The results indicate that the methods described here can provide heat transport estimates with a maximum uncertainty of ± 0.18 PW ($1\,\text{PW} = 10^{15}\,\text{W}$). Most of this uncertainty is due to the climatology used to estimate the deep structure and issues related to not knowing the absolute velocity field and most especially characterizing barotropic motions. Nevertheless, when the methodology is applied to temperatures collected along 30°S (A10) and direct model integrations, the results are very promising. Results from the numerical model suggest that ageostrophic non-Ekman motions can contribute less than 0.05 PW to heat transport estimates in the South Atlantic.
Published by Elsevier Ltd.

1. Introduction

One of the goals in the global ocean observing system is to accurately describe the strength of the meridional overturning circulation (MOC), the vigorous circulation that redistributes heat, nutrients, carbon and fresh water globally. In the South Atlantic, the MOC is composed of northward transport of warm surface and intermediate layer waters in the upper 1200 m, southward transport of North Atlantic Deep Water (NADW) between approximately 1200 and 4000 m, and northward flowing Antarctic Bottom Water (AABW) below 4000 m. Within the subtropical region, in the

*Corresponding author. Tel.: +1 305 361 4338; fax: +1 305 361 4392.
E-mail addresses: Molly.Baringer@noaa.gov (M.O. Baringer), Silvia.garzoli@noaa.gov (S.L. Garzoli).

0967-0637/$ - see front matter Published by Elsevier Ltd.
doi:10.1016/j.dsr.2007.03.011

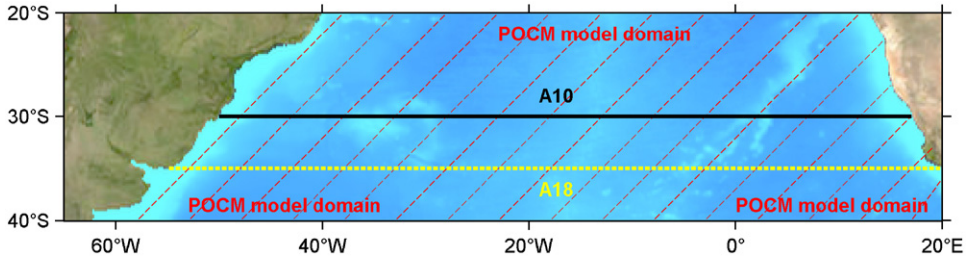

Fig. 1. Map of A10 location, XBT locations, POCM area with the main circulation elements schematically drawn (see text).

30–35°S band, historical heat transport estimates range from small southward values (e.g., −0.23 PW, de las Heras and Schlitzer, 1999) to close to 1 PW northward (0.88 PW, inverse model, Fu, 1981). To see the large range in various estimates of South Atlantic heat transport see Fig. 13. in Garzoli and Baringer (2007). Note that large heat transport variability may be a real feature of the South Atlantic circulation because both margins are highly energetic and the winds are variable.

The 'best-practices' method for estimating the net meridional transports typically includes the costly and time-consuming full-water-column, cross-basin hydrographic section. Such full-depth sections have been used with the geostrophic method to estimate the strength of the meridional heat transport at many locations. Direct estimates of the meridional heat transport in the South Atlantic have include Holfort and Siedler (2001), Saunders and King (1995) and Talley (2003). More involved estimation methods have included using more than one section and using observed velocities to constrain the circulation (e.g., Macdonald et al., 2001; Ganachaud and Wunsch, 2003).

Partly because of the expense of these 'best-practices' sections, other observations systems were envisioned to measure parts of the MOC in hopes of capturing some aspects of its variability. In particular, expendable bathythermographs (XBTs) deployed in cross-basin (full-width), relatively closely spaced (high-density) sections were conceived to measure the mesoscale variability at higher frequencies than one can afford to occupy full basin sections and thus the XBT sections can help assess whether unusual circulation features are present that could bias estimates based on a single full-depth section (Smith et al., 1999). Roemmich et al. (2001) demonstrated that XBTs could also successfully be used to estimate the meridional transport in the North Pacific. They estimated the net heat transport by specifically prescribing the transport below the deepest level of the XBT observations. In this paper, we will develop a methodology to calculate directly the deep transports using climatological data. In particular, the high-density XBT line called AX18 is used as an example XBT section where this method could be applied. The AX18 line, between Cape Town, South Africa, and Buenos Aires, was designed to monitor the upper-layer mass budget in the South Atlantic and to estimate the variability of the upper limb of the MOC transport. We evaluate the method against the full-depth, complete hydrographic section taken during the World Ocean Circulation Experiment (WOCE), the 30°S A10 section, in the same region. Errors are also estimated by analyzing the output of a numerical model simulation of the South Atlantic taken from the Princeton Ocean Circulation Model (Tokmakian and Challenor, 1999). The locations of the sections used in this paper are shown in Fig. 1.

2. Data and methodology

Direct estimates of meridional volume (V) mass (M) and heat (H) transport require the knowledge of the potential temperature (T), salinity (S) and meridional velocity (v) fields:

$$V = \int\int v\,dx\,dz \quad \left[\mathrm{Sv} = 10^6\,\mathrm{m^3\,s^{-1}}\right],$$

$$M = \int\int \rho v\,dx\,dz \quad \left[\mathrm{kg/s}\right],$$

$$H = \int\int \rho c_p T v\,dx\,dz \quad \left[\mathrm{PW} = 10^{15}\,\mathrm{W}\right],$$

where ρ is the density of the water and c_p the specific heat capacity.

The total meridional velocity (v) can be decomposed into three components:

$$v = v_g + v_{ag} + v_b,$$

where v_g is the geostrophic (baroclinic) component, which can be estimated from the hydrographic field, v_b is the barotropic component (here defined as the reference velocity used to make v_g absolute), and v_{ag} is the ageostrophic component, which is assumed to be dominated by the wind-forced Ekman transport. Meridional Ekman transports are computed as the Ekman mass, M_y, and Ekman heat, H_y, transport given by

$$M_y = -\frac{\tau_x}{f}\Delta x,$$

$$H_y = M_y c_p T_{EK},$$

where τ_x is the zonal component of the wind stress, f is the Coriolis parameter, Δx is the horizontal distance and T_{EK} is the mean temperature of the Ekman layer.

The methodology used to obtain the baroclinic component of the heat transport from the XBT data collected along AX18 is as follows: the XBT data are collected using an automated launcher, with a Sippican MK 12 circuit board and GPS receiver that stores 6–8 XBT records from deployments at specified time or space intervals. XBT data from Sippican T-7 XBTs consist of temperature time series collected every 0.1 s that typically extend to depths of about 850 m. The temperature time series is then converted into a depth profile using the updated fall-rate equation of Hanawa et al. (1995). In this paper, salinity (S) is estimated for each XBT profile by using S (T, P, latitude, longitude) derived from ARGO and CTD data following the methodology described by Thacker (2007a, b). The XBT probe samples the ocean only to a depth of about 850 m. Meaningful heat transport estimates require full-water-column properties. Hence, a two-dimensional interpolation of the high resolution (0.25°) temperature and salinity climatology produced by Boyer et al. (2006) to the location of each XBT, at each depth level, is used to generate an annual mean climatology for the deep ocean. The bottom is determined to be the depth at the location of the XBT from the Smith and Sandwell (1997) two-minute bathymetry database. Sections must span the entire ocean basin so as to conserve mass. Typically, WOCE specifications require samples up to the 200 m isobath: sections that reach this close to the coastlines are considered "complete". Note that there may be some flow along the shelves shallower than 200 m. Appendix A describes some of these flows which can lead to a mass uncertainty of 0–0.2 Sv and a heat transport uncertainty of up to 0.01 PW. These uncertainties have been added to the total one on Table 3.

Geostrophic velocities are determined using the dynamic method where a level of no motion was chosen at $\sigma_2 = 37.09\,kg\,m^{-3}$ (σ_2 defined as potential density relative to 2000 dbar) to compare with results from Ganachaud and Wunsch (2003). Ekman transports are determined using national centers for environmental prediction (NCEP) monthly reanalysis winds by interpolating the NCEP values to the location of the XBT observations. The monthly NCEP reanalysis winds were provided by NOAA-CIRS Climate Diagnostic Center, via their web site at http://www.cdc.noaa.gov. Transports are computed in layers and summed for the entire water column. The initial level of no motion velocity field is uniformly adjusted so that the net salt transport across the section matches the salt flux through the Bering Straits ($27.6 \times 10^6\,kg\,s^{-1}$, Coachman and Aagaard, 1988). Typically, values of this velocity are in the range of 10^{-4} to $10^{-6}\,m\,s^{-1}$ and hence there is, strictly speaking, only a level of prescribed motion.

3. Heat transports across 30°S

The method described in the previous section can be applied to the 30°S WOCE CTD section by successively degrading the CTD observations until they finally appear at if the original data were nothing more than 850-m XBTs. This exercise assures us that the geostrophic method is appropriate for the region and generates error estimates for each of the assumptions applied to actual XBT data to generate an estimate of the additional uncertainty that arises from having only XBT data.

The WOCE A10 CTD section was conducted nominally along 30°S during January 1993, and provided temperature and salinity as a function of depth for the whole water column across the entire South Atlantic Ocean (Fig. 2). Ganachaud and Wunsch (2003) analyzed the 30°S CTD data using the geostrophic method, with absolute velocity corrections applied based on an inverse model, to estimate the meridional heat transport across 30°S. They used a deep reference level approximately between AABW and NADW along a neutral density of 28.11 (equivalent to $\Theta \sim 1.9\,°C$ or $\sigma_2 = 37.09\,kg\,m^{-3}$), and constrained the solution to have 7 ± 2 Sv of AABW flowing north in the western basin and to have 0 ± 2 Sv flowing north from below approximately 4000 m east of 7°W. Fig. 2

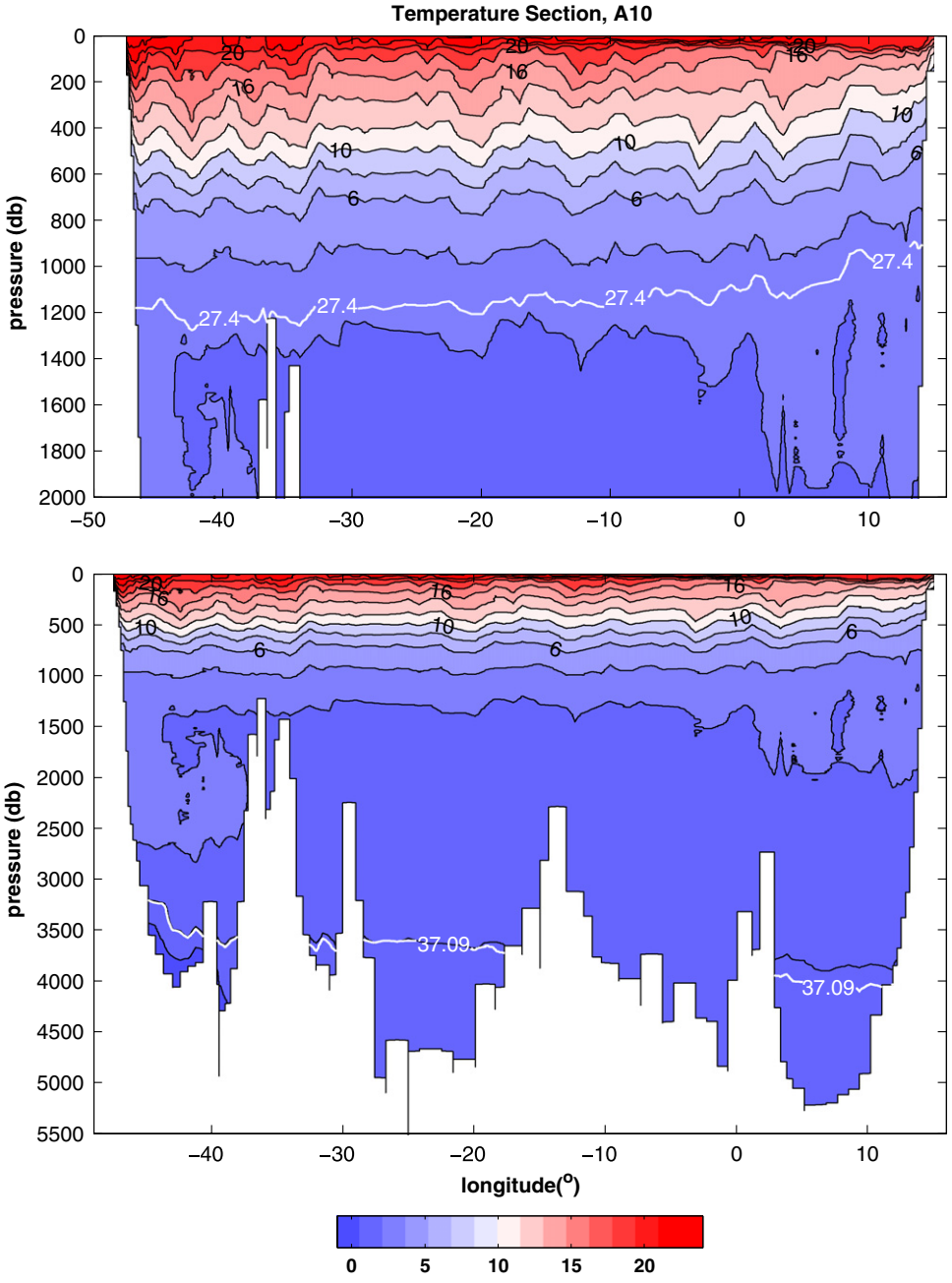

Fig. 2. Temperature section from the data collected along the WOCE 30°S CTD line A10. White lines represent important density surfaces: 27.4 kg m^{-3} represents the upper boundary of intermediate water and 37.09 kg m^{-3} is the reference level used for transport calculations (the lower boundary of NADW).

shows the vertical distribution of temperature and the density levels from 30°S CTD data. To calculate the Ekman transport, Ganachaud and Wunsch (2003) used annual mean NCEP climatological winds and found a total heat transport of 0.4 PW. More recently McDonagh and King (2005), using a box inverse model, recalculated the heat flux across 30°S (A10) and obtained the value of 0.22 ± 0.08 PW, a number the authors considered to be in agreement with previous results.

The simple geostrophic method described in the previous section is applied to the full-water-column

Table 1
Heat transport estimates for the WOCE 30°S CTD section (A10) using (1) Ganachaud and Wunsch (2003) inverse method, (2) direct estimates of geostrophic transports, (3) in the upper 850 m, CTD temperatures collected during A10, salinities estimated using the methodology proposed by Thacker (2007a, b) and (4) same as 3 but below 850 m the data is from the 0.25° climatology (Boyer et al., 2006)

	Source	Heat transport (PW)
1	Ganachaud and Wunsch (2003)	0.40
2	Direct estimate	0.40
3	Above 850 m, T from A10, S estimated	0.43
4	Climatology below 850 m	0.55

values of $T(z)$ and $S(z)$ collected along 30°S (A10) to obtain direct estimates of heat transport. Results are given in Table 1. A comparison between the results obtained by Ganachaud and Wunsch (2003) (0.40 PW, Table 1, line 1) and those obtained by the simple geostrophic method using T and S data from A10 (0.40 PW, Table 1, line 2) indicates that the basic methodology applied herein reproduces the values obtained with the inverse method.

XBTs, however, contain no salinity information. This deficiency can be simulated with WOCE A10 CTD data, by considering the $T(z)$ values from A10, and prescribing the salinity above 850 m from the functions of temperature, depth and geographic location provided by Thacker (2007a, b). Thacker (2007a, b) created salinity look-up tables for the region under study based on ARGO & CTD data relations between T and S as a function of latitude, longitude and pressure. Below 850 m the full 30°S CTD data set is used. Heat transport obtained this way is computed as 0.43 PW (results in Table 1, line 3). Thus, the error induced by estimating salinities with the functions provided by Thacker is very small (less than 0.03 PW, "Upper Ocean Salinity", Table 3).

XBTs sample only the upper 850 m of the water column and hence some estimate of the deeper values must be made. WOCE A10 CTD data is used such that $T(z)$ above 850 m is obtained directly from the CTD data. Salinity above 850 m is inferred using the relations provided by Thacker (2007a, b). Below 850 m the World Ocean Atlas 0.25° annual mean $T(z)$ and $S(z)$ fields are used (WOA0.25). Heat transport is estimated as 0.55 PW following the previously described methodology (results in Table 1, line 4). In this case, there is a difference of +0.15 PW ("Deep Climatology", Table 3).

Using full-water-column CTD data, the depth at any location is typically known to within about 10 m. With XBTs the depth must be determined from the Smith and Sandwell (1997) database. Using the CTD data as if it were an XBT, and the depth as determined from Smith and Sandwell instead of the maximum depth provided by the CTD cast, it was determined that the error introduced by not knowing the exact water depth is on the order of 0.02 PW ("Bottom depth", Table 3).

The methodology used here requires the salt to exactly balance the salt transport through the Bering Strait following Coachman and Aagaard (1988). The salt conservation constraint results in a small residual mass flux of 0.3 Sv to the south that results from the 0.8 Sv flow through the Bering Straits (Coachman and Aagaard, 1988). For the numerical model analysis, the mass residual ranged from 0.3 to 0.5 Sv southward. We assume that our top to bottom net mass transports are accurate to about 1 Sv, hence this mass residual plays no significant role in the circulation, however, a small error in the estimated heat transport will arise. An upper bound on this error would occur is the mass was carried entirely in the near surface with temperatures between 14 and 22 °C. The additional uncertainty in the heat transport would thus be less than 0.02 PW ("Mass imbalance", Table 3).

Results from this analysis are represented graphically in Fig. 3, showing the cumulative heat transport across the basin along constant latitude similar to the WOCE A10 section. The thin dashed line is the cumulative heat transport in PW obtained from the observed $T(z)$ and $S(z)$ collected at the CTD stations occupied during A10. The thick solid line is the cumulative heat transport obtained from the $T(z)$ values of A10 above 850 m, using salinities above 850 m from Thacker (2007a, b) methodology and $T(z)$ and $S(z)$ below 850 m obtained by using the values of the WOA0.25 climatology. The main variability across the basin is reproduced accurately using only the upper 850 m of data. Thus, it can be concluded that the methodology proposed herein can reproduce the variability in heat transport as obtained with the inverse method, and furthermore that when heat transports are computed from simulated XBT profiles collected in the upper 850 m, there is an uncertainty of 0.15 PW in the cumulative transport across the basin due to the assumptions specific to using only XBT profiles instead of full-water-column CTD profiles. Of

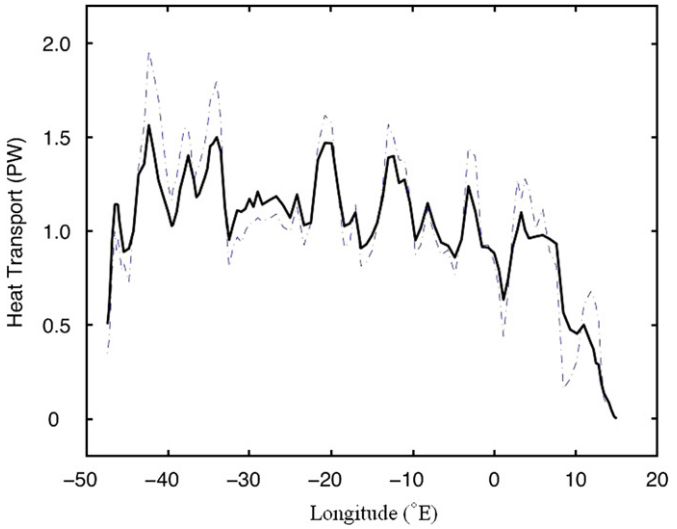

Fig. 3. Cumulative heat transport across 30°S. The thin dashed line is the cumulative heat transport obtained from the $T(z)$ and $S(z)$ collected along the WOCE CTD section (A10). The thick solid line is the cumulative heat transport obtained from the $T(z)$ values of A10 above 850 m, salinities above 850 m obtained using Thacker (2007a, b) methodology and $T(z)$ and $S(z)$ below 850 m from the high-resolution (0.25°) climatology (Boyer et al., 2006). Ekman transport is obtained using NCEP annual mean winds. The agreement between the two curves supports the validity of the proposed methodology.

course this analysis is based on a single section because no other is available close to the location of the XBT line AX18 for which this error estimate is based. However, in the North Atlantic near the high-density XBT line AX7 (not shown), five CTD sections have been conducted along 24°N and a similar analysis there indicates no mean bias to the XBT heat transport estimates and similar scatter for individual estimates as shown here.

4. Heat transports from a model

Additional uncertainties in the results may be due to the simplicity of the geostrophic method that applies to any hydrographic section (e.g., Ganachaud and Wunsch, 2003) as well as to our results. In particular, the role of the barotropic and ageostrophic components of the flow and the very time-dependent nature of the flow lead to additional uncertainty. In what follows, the POCM numerical model (Tokmakian and Challenor, 1999) is examined to compare results estimated from the total velocity field to those obtained from geostrophic velocities. This model was chosen because it is one of the most well-known and thoroughly tested eddy-permitting ocean general circulation models around. It has been analyzed and compared to observations by numerous investigators (e.g., Stammer et al., 1996; Gille, 1997 ; Matano and Beier, 2003) and we believe it captures most of the processes in play in the South Atlantic.

4.1. Estimates of the total heat transport using the velocity field from the model

From the model velocity field, the heat transports are computed for model latitudes 29.96°S (nominally 30°S) and 35.05°S (nominally 35°S) (Fig. 4). The time series of heat transport for the model years 1986–1998 (the year when the WOCE A10 line was conducted) indicate a strong interannual variability with values between 0.2 and 1.2 PW. The mean value of the series is 0.55 PW at 30°S and 0.60 PW at 35°S with standard deviations of 0.24 PW and 0.28, respectively (Table 2). The model mean annual cycle exhibits a maximum (0.76 PW at 30°S and 0.84 PW at 35°S) in the month of July and a minimum (0.42 PW at 30°S and 0.46 PW at 35°S) in the month of February (Fig. 4), and explains 31% of the total variance at 30°S and 17% of the total variance at 35°S. Note that the WOCE A10 section was occupied during the climatological low point in the model seasonal cycle (January), and hence the heat transports from A10 are consistent with the POCM model. The vertical distributions of the volume and heat transports indicate that all of the northward flow is contained in the upper 1335 m of the ocean (Fig. 5). The model also shows that

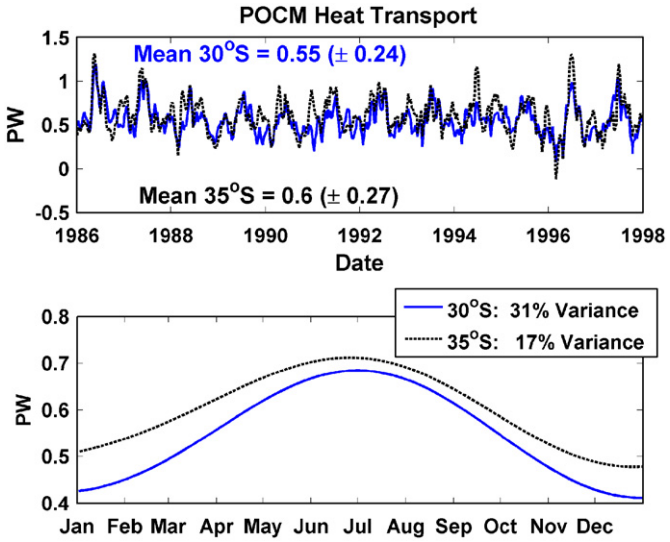

Fig. 4. Time series of the total heat transport (top panel) at 30°S (solid) and 35°S (dashed) obtained from the POCM velocity and temperature fields. In parenthesis after the mean value of the series is the standard deviation. The lower panel is the climatological annual cycle of the heat transport (1986–1998) computed from the full-time series at 30°S (represents 31% of the RMS variance) and at 35°S (represents 17% of the RMS variance).

Table 2
Results from the analysis of the POCM model

	Results from the POCM analysis	Heat transport (PW)			
		Latitude model section			
		30°S		35°S	
		Mean	SD	Mean	SD
A	Direct calculation (from model velocity field)	0.55	0.24	0.60	0.28
	Geostrophic Tr using model V as reference level	0.49	0.16	0.64	0.18
	Mean difference (ageostrophic component)	0.06	0.18	−0.04	0.2
B	Direct calculation (from model velocity field)	0.55	0.24	0.60	0.28
	Geostrophic Tr using $\sigma_2 = 37.09\,\mathrm{kg\,m^{-3}}$as reference level	0.67	0.14	0.62	0.15
	Mean difference (ageostrophic component)	−0.12	0.21	−0.02	0.28
C	Direct calculation (from model velocity field)	0.55	0.24	0.60	0.28
	Same as 2 using mean V at the western boundary	0.6	0.14	0.55	0.15
	Mean difference (ageostrophic component)	−0.05	0.19	0.05	0.25

A: Comparison between the results from direct calculation of the transport using the model velocities and from the geostrophic method using the model velocity to determine the reference level at all locations. B: Comparison between the results from direct calculation of the transport using the model velocities and from the geostrophic method with $\sigma_2 = 37.09\,\mathrm{kg\,m^{-3}}$ as reference level. C: Comparison between the results from direct calculation of the transport using the model velocities and from the geostrophic method with $\sigma_2 = 37.09\,\mathrm{kg\,m^{-3}}$ as reference level and a mean bottom velocity in the western boundary. Note the values quoted are for the model grid points at located at −30.13°S and −35.195°S.

there are relatively small variations in the heat transport in the latitude range between 30°S and 35°S (Fig. 6). Between 30ºS and 35ºS the model heat transport changes by about 0.05 PW over an area of approximately $4 \times 10^{12}\,\mathrm{m^2}$ suggesting a small heat convergence in this region. This heat convergence is equivalent to about $11\,\mathrm{W\,m^{-2}}$ heat loss to the atmosphere. However, estimates of net surface heat fluxes remain much larger than this, for example, Josey et al. (1999) estimate a global

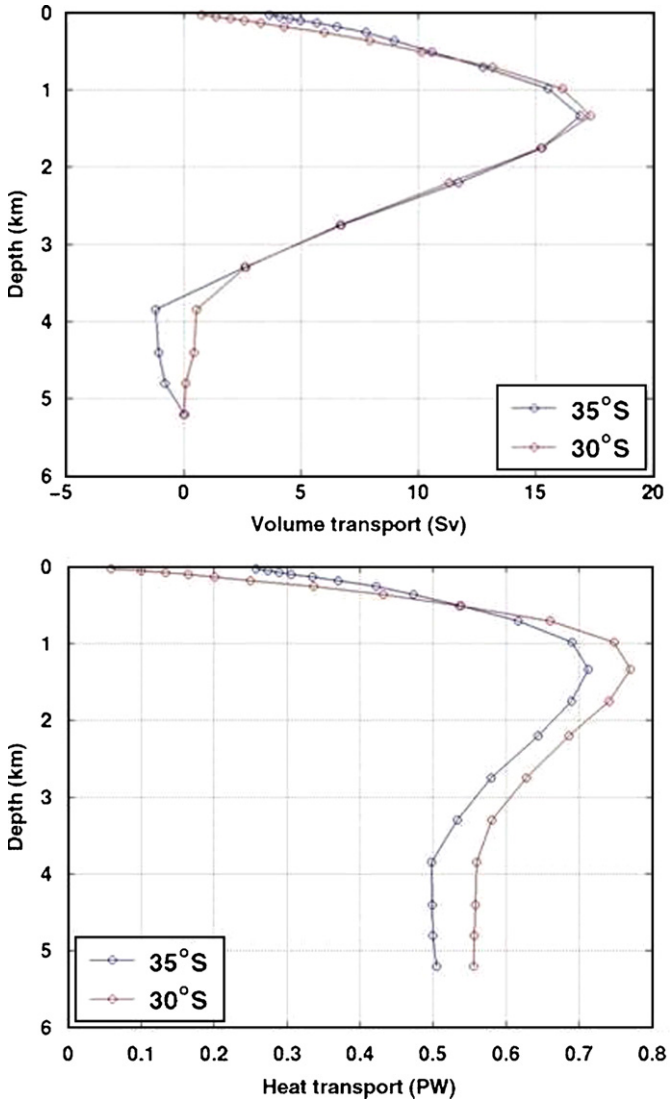

Fig. 5. Cumulative vertical distribution of MOC volume transport (top) and heat transport (bottom) from the POCM model.

accuracy of $30\,W\,m^{-2}$ and hence these differences are considered negligible.

4.2. Estimates of the model ageostrophic component of the flow

The total transport is equal to the geostrophic plus the ageostrophic components of the flow. It is currently assumed that the major contributor to the ageostrophic field is the Ekman flow induced in the upper layer by the winds. Other processes may also contribute to the heat transport, such as inertial motions and eddy fluxes. To estimate the magnitude of the non-Ekman ageostrophic components of the flow, the model, which is one estimate of the total transport, can be analyzed using the simple steady geostrophic method. Differences between the total model transport obtained from the model velocity field (''direct calculation'', Table 2) and the geostrophic method must be some combination of methodological errors and non-Ekman ageostrophic transports. The best estimate of the geostrophic component of the flow is computed from the model temperature and salinity using as a reference level the model velocity field at a prescribed depth. This estimate should eliminate methodological errors due to referencing because the actual model velocities at depth are given. The Ekman component of the flow is calculated from the ECMWF winds for consistency with the model

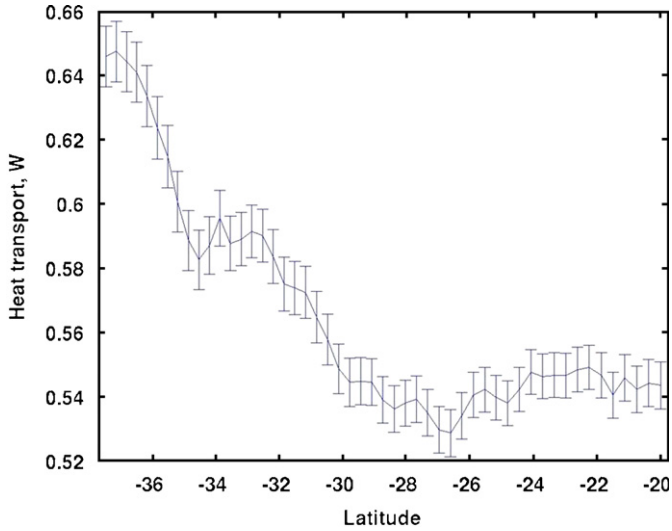

Fig. 6. Heat transport from the POCM model as a function of latitude.

runs. The geostrophic-method heat transport is determined from the geostrophic velocity field modified to include the ageostrophic Ekman velocity. Then the mean ageostrophic (non-Ekman) component of the model heat transport is estimated as the difference between the total heat transport (computed directly from the model velocity field) and the geostrophic-method heat transport. Results indicate (Table 2) that at 30°S the mean ageostrophic (non-Ekman) component of the heat transport is 0.06 PW and, at 35°S −0.04 PW. The standard deviations of these new estimates of geostrophic heat transport have also significantly decreased to 0.16 PW at 30°S and 0.18 PW at 35°S, from 0.24 PW at 30°S and 0.28 PW at 35°S obtained from the direct model integration. This may indicate of the presence of ageostrophic time-dependent shear in the full model fields that is not present in the geostrophic estimates. Given the small values of the mean difference and the large standard deviations (0.18 PW at 30°S and 0.20 PW at 35°S), these values are not statistically significantly different from zero, and hence for a long-term mean geostrophic heat transport estimates will work quite well (i.e., better than about ±0.05 PW, "Ageostrophic non-Ekman" error, Table 3).

Table 3
Error estimates for the heat transport values

Uncertainty estimate	PW
Upper ocean salinity	0.03
Deep climatology below 850 m	0.15
Bottom depth	0.02
Mass imbalance	0.02
Western boundary mean velocity	0.02
Ekman	0.04
Unresolved shelf transport	0.01
Ageostrophic non-Ekman	0.05
Ring transport	0.02
Reference level	0.05
Total	0.18

4.3. Errors due to rings

It is important to note that there may still be contributions to the heat transport from time-dependent eddy fluxes or transients. In the case of the region under consideration, these sort of motions may include the ring shedding both at the retroflection of the Agulhas Current on the eastern side of the basin, or at the confluence of the Brazil and Malvinas Currents on the western side. Note that the geostrophic estimate of the heat transport from temperature and salinity is just a snapshot of the flow at a simple point in time that may or may not have captured an Agulhas ring. From rings surveyed during the Benguela Current Experiment, Garzoli et al. (1999) calculated a mean heat transport per ring of 0.003 PW and from altimetric estimates, 0.004 PW. Goñi et al. (1997) calculated that on average five Agulhas rings enter the Atlantic each year. If all the rings move north across the section, this could account for an average of 0.02 PW per year, a number similar to the mean ageotrophic non-Ekman flow in the model ('Ring transport', Table 3).

4.4. Errors in reference velocity

The model can further be used to estimate the importance of barotropic motions in the region by comparing the model heat transports (as in part a, above) with possible reference level choices. The geostrophic transports are calculated using the T and S fields from the model output by applying the geostrophic method previously described and using as reference level $\sigma_2 = 37.09\,\mathrm{kg\,m^{-3}}$ (note than in the previous exercise reference level was determined by actual model values of velocity). Differences between the heat transports from the total velocity and from the geostrophic method, for reference level $\sigma_2 = 37.09\,\mathrm{kg\,m^{-3}}$, are -0.12 PW at 30°S and -0.02 PW at 35°S (Table 2). These results indicate that there is a small component of the flow (between 0.02 and 0.12 PW, depending on the latitude) that is not taken into account using a simple uniform reference velocity on a single surface. Through further inspection of the model fields, a barotropic component was observed west of 45°W, with southward bottom velocities having a mean of $0.06\,\mathrm{m\,s^{-1}}$. This barotropic flow is the result of the Brazil Current and the NADW flowing in the same direction. When the heat transport values obtained from the T and S are corrected for the barotropic component of the flow (by adding a mean bottom velocity in the western boundary of $-0.032\,\mathrm{m\,s^{-1}}$ at 30°S and $-0.013\,\mathrm{m\,s^{-1}}$ at 35°S for all station pairs west of 45°W), results for the heat transport are 0.60 PW at 30°S and 0.55 PW at 35°S (Table 2), similar to the ones obtained by using the model velocity field. That is to say, a more accurate mean value for the heat transport from the data collected along AX18 may be obtained by correcting for the barotropic component of the field at the western boundary (0.05 PW "Reference level" error, Table 3).

5. Discussion and conclusions

The heat transport estimates contained herein are subject to uncertainties that can broadly be divided into two categories: those arising from using XBTs instead of full-water-column hydrographic profiles and those uncertainties inherent in any heat transport estimate based on hydrographic data. In the previous section, where we verified the accuracy of the geostrophic method using XBTs, three main issues arose: estimating salinity, estimating the deep climatology and estimating the true bottom depth. A summary of these transport uncertainties is given in Table 3. We found a heat transport uncertainty of 0.03 PW arising from estimating the salinity. The use of a smooth climatology for the lower layers introduces an uncertainty of 0.15 PW to the heat transport estimates, which we assume is a bias due to the smoothed nature of the deep fields "smearing out" density gradients that should carry the lower limb of the MOC through geostrophic shear, and the uncertainty about the depth of the bottom of the ocean introduces an error of 0.02 PW.

All heat transport estimates also suffer from uncertainties associated with the determination of the absolute circulation. For instance, uncertainties arise from the known variability in the western boundary bottom velocities: examination reveals that by increasing the bottom reference velocity, v by as much as $\pm 20\%$, the heat transport varies by only ± 0.02 PW, an uncertainty due to not knowing the true mean western boundary reference velocity (Table 3, 'western boundary mean velocity'). Different wind products produce Ekman heat transport values that differ by about ± 0.04 PW (Table 3, 'Ekman'). Unresolved shelf transport is noted in Appendix A and can result in heat transport uncertainty of 0.01 PW (Table 3, 'unresolved shelf transport'). Ageostrophic motions and reference level errors are estimated using the POCM model: ageostrophic motions not associated with Ekman transports can add an uncertainty of 0.05 PW (Table 3, 'ageostrophic non-Ekman'). Not knowing the true absolute velocity field adds an additional uncertainty of 0.05 PW (Table 3, 'reference level'). A summary of all estimated uncertainties is given in Table 3. The total uncertainty is thus estimated to be ± 0.18 PW.

In summary, the methodology used to obtain the heat transport was examined in detail using several "test" cases as benchmarks. It was shown that the method could essentially reproduce the values obtained using more sophisticated data and analysis with the WOCE hydrographic line A10 along 30°S. The analysis of the product of a numerical model confirmed that baroclinic estimates of the transports should be adjusted by the contribution of a strong barotropic component of the flow along the western boundary. It was also shown that replacing the A10 hydrographic section below 850 m (the deepest values of data collected with XBTs) with climatological fields introduces a change of $+0.15$ PW to the heat transport, which was listed as an additional uncertainty in the heat-transport estimates. When

comparing to other estimates, it is possible that a positive bias has been introduced into our estimates due to the methodology of using a smoothed deep-water climatology, and therefore our estimates may be slightly high. However, an annual mean climatology has been used, and hence all the variability in heat transport is entirely due to the changing thermal structure of the upper water column, plus wind and boundary current changes. The data collected by Argo profiling floats helped to improve the T/S relations in the region, but better subsurface climatology for the lower layers is needed in order to improve the results.

Acknowledgements

This work would not have been possible without the support of Ms. Qi Yao, for help with calculations used in this paper. Dr. Carlisle Thacker provided the T/S relations for the region. Dr. Ricardo Matano graciously provided the model output and many useful comments to this manuscript and throughout the analysis. Roberta Lusic prepared the manuscript for publication. This work is supported by the Office of Climate Observations and the National Oceanic and Atmospheric Administration.

Appendix A. Continental shelf transport

Note that there is always a small portion of the flow on the continental shelf that is not captured by the measurements. Along the western boundary, Palma et al. (2004) conducted a careful analysis of the currents along the Argentine continental shelf. They analyzed the modeled oceanic circulation patterns on the shelf forced by nine different wind climatologies. Results indicate that at 35°S there is a weak northward transport that varies between 0.0 and 0.2 Sv, depending on the wind climatology. A shelf flow of 0.2 Sv introduces a change in the heat transport of less than ± 0.01 PW (Table 3, "unresolved shelf transport"), a value that is less than the other uncertainties.

Along the eastern shelf, Bang and Andrews (1974), using direct current measurements, found a strong equatorward jet along the inner shelf of South Africa southwest of Cape Town, confined to the mid-depth and surface layers and with a width of 5 nautical miles. According to Shannon and Nelson (1996), the estimated mean transport of this current is 1 Sv. Compensating for the vertical displacement of water on the inner shelf and its movement northward is a narrow strip of southward flow found at the base of the shelf (Nelson, 1989, 1991). This poleward flow is part of a more extensive poleward motion stretching from the coast across the shelf and out into the Cape Basin to as far as 17° 35′E (Shannon and Nelson, 1996; Nelson, 1989). South of 33°S, the flow is not seasonally dependent. The net contribution to the heat transport from the coast to 17.5°E is negligible because of the compensating northward and southward coastal currents (Nelson, 1989). An extremely conservative estimate of the mean temperature differences between these currents (5 °C) leads to an estimated heat transport of less than 0.01 PW.

References

Bang, N.D., Andrews, W.R.H., 1974. Direct current measurements of a shelf-edge frontal jet in the southern Benguela system. Journal of Marine Research 32, 405–417.

Boyer, T., Levitus, S., Garcia, H., Locarnini, R., Stephens, C., Antonov, J., 2006. Objective analyses of annual, seasonal and monthly temperature and salinity for the World Ocean on a 1/4 degree grid. International Journal of Climatology 25, 931–945.

Coachman, L.K., Aagaard, K., 1988. Transports through Bering Strait: annual and interannual variability. Journal of Geophysical Research 93, 15535–15539.

de las Heras, M.M., Schlitzer, R., 1999. On the importance of intermediate water flows for the global ocean overturning. Journal of Geophysical Research 104, 15515–15536.

Fu, L.L., 1981. The general circulation and meridional heat transport of the subtropical south Atlantic determined by inverse methods. Journal of Physical Oceanography 11, 1171–1193.

Ganachaud, A.S., Wunsch, C., 2003. Large-scale ocean heat and freshwater transports during the World Ocean Circulation Experiment. Journal of Climate 16, 696–705.

Garzoli, S.L., Baringer, M.O., 2007. Meridional heat transport using expandable bathythermographs. Part II: South Atlantic Transport. Deep Sea Research Part I, in press, doi:10.1016/j.dsr.2007.04.013.

Garzoli, S.L., Richardson, P.L., Duncombe Rae, C.M., Fratantoni, D.M., Goni, G.J., Roubicek, A.J., 1999. Three Agulhas rings observed during the Benguela current experiment. Journal of Geophysical Research 104, 20971–20985.

Gille, S., 1997. The southern ocean momentum balance: evidence for topographic effects from numerical model output and altimeter data. Journal of Physical Oceanography, 2219–2232.

Goñi, G.J., Garzoli, S.L., Roubicek, S.L., Olson, A.J., Brown, D.B., 1997. Agulhas ring dynamics from TOPEX/POSEIDON satellite altimeter data. Journal of Marine Research 55, 861–883.

Hanawa, K., Rual, P., Bailey, R., Sy, A., Szabados, M., 1995. A new depth-time equation for Sippican or TSK T-7, T-6 and T-4 expendable bathythermographs (XBT). Deep Sea Research I (42), 1423–1451.

Holfort, J., Siedler, G., 2001. The Meridional oceanic transports of heat and nutrients in the south Atlantic. Journal of Physical Oceanography 31, 5–29.

Josey, S.A., Kent, E.C., Taylor, P.K., 1999. New insights into the ocean heat budget closure problem from analysis of the SOC air-sea flux climatology. Journal of Climate 12, 2856–2880.

Macdonald, A.M., Baringer, M.O., Ganachaud, A., 2001. Heat transport and climate. Encyclopedia of Ocean Sciences 2, 1195–1206.

Matano, R.P., Beier, E.J., 2003. A kinematic analysis of the Indian/Atlantic interocean exchange. Deep Sea Research Part II: Topical Studies in Oceanography 50 (1).

McDonagh, E.L., King, B.A., 2005. Oceanic fluxes in the south Atlantic. Journal of Physical Oceanography 35, 109–122.

Nelson, G., 1989. Poleward motion in the Benguela area. In: Neshyba, S.J., Mooers, C.N.K., Smith, R.L., Barber, R.T. (Eds.), Poleward Flows along Eastern Ocean Boundaries, Coastal and Estuarine Studies, vol. 34. Springer, New York, pp. 110–130.

Nelson, G., 1991. An equatorward jet wash of Cape Town. Abstract IAPSO Proceedings XX Assembly Vienna, p. 189.

Palma, E.D., Matano, R.P., Piola, A.R., Sitz, L.E., 2004. The impact of wind climatologies on the modeled barotropic circulation of the Southwestern Atlantic Continental Shelf. Geophysical Research Letter, 31, L24303, doi:10.1029.

Roemmich, D., Gilson, J., Cornuelle, B., Weller, R., 2001. Mean and time-varying meridional transport of heat at the tropical/subtropical boundary in the North Pacific Ocean. Journal of Geophysical Research 106 (C5), 9255–9275.

Saunders, P.M., King, B.A., 1995. Oceanic fluxes on the WOCE A11 section. Journal of Physical Oceanography 25, 1942–1958.

Shannon, L.V., Nelson, G., 1996. The Benguela: large scale features, process and system variability. In: Wefer, G., Berger, W.H., Siedler, G., Webb, D.J. (Eds.), The South Atlantic: Past and Present Circulation. Springer, New York, pp. 163–210.

Smith, W.H.F., Sandwell, D.T., 1997. Global seafloor topography from satellite altimetry and ship depth soundings. Science 277, 1957–1962.

Smith, N.R., Harrison, D.E., Bailey, R., Alves, O., Delcriox, T., Hanawa, K., Keeley, B., Meyers, G., Molinari, B., Roemmich, D., 1999. The role of XBT sampling in the ocean thermal network. In: The Ocean Observing System for Climate: Ocean Obs 99(1).

Stammer, D., Tokmakian, R., Semtner, A., Wunsch, C., 1996. How well does a 1/4° global circulation model simulate large-scale oceanic observations & quest. Journal of Geophysical Research 101 (C11), 25779–25812.

Talley, L.D., 2003. Shallow, intermediate, and deep overturning components of the global heat budget. Journal of Physical Oceanography 33, 530–560.

Thacker, W.C., 2007a. Estimating salinity to complement observed temperature: Part 1: Gulf of Mexico. Journal of Marine Science 65/1–4, 224–248.

Thacker, W.C., 2007b. Estimating salinity to complement observed temperature: 2. Northwestern Atlantic. Journal of Marine Systems. 65/1–4, 249–267. DOI information: 10.1016/j.jmarsys.2005.06.007.

Tokmakian, R.T., Challenor, P.G., 1999. On the joint estimation of model and satellite sea surface height anomalies. Ocean Modelling 1, 39–52.